Published on 16 September 2015. Downloaded by State Public Scientific Technical Library, Siberian Branch of the RAS on 10/19/2020 12:44:16 PM.

Dalton Transactions

PAPER

View Article Online
View Journal | View Issue

Cite this: *Dalton Trans.*, 2015, **44**, 18078

# Effects of composition modulation on the luminescence properties of $Eu^{3+}$ doped $Li_{1-x}Ag_xLu(MoO_4)_2$ solid-solution phosphors†

Fangrui Cheng,[a] Zhiguo Xia,*[a,b] Maxim S. Molokeev[c,d] and Xiping Jing[e]

Received 20th July 2015,
Accepted 16th September 2015

DOI: 10.1039/c5dt02760h

www.rsc.org/dalton

Double molybdate scheelite-type solid-solution phosphors $Li_{1-x}Ag_xLu_{1-y}(MoO_4)_2:yEu^{3+}$ were synthesized by the solid state reaction method, and their crystal structures and luminescence properties were investigated in detail. The composition modulation and structural evolution of this series of samples were studied and the selected $AgEu(MoO_4)_2$, $AgLu(MoO_4)_2$, $LiLu(MoO_4)_2$ and $LiEu(MoO_4)_2$ phases were analyzed based on the Rietveld refinement. Depending on the variation of the Li/Ag ratio in $Li_{1-x}Ag_xLu_{1-y}(MoO_4)_2:yEu^{3+}$ phosphors, the difference in the luminescence properties of $Li_{1-x}Ag_xLu_{1-y}(MoO_4)_2:yEu^{3+}$ phosphors was ascribed to two factors, one reason could be assigned to the coupling effect and the nonradiative transition between the energy levels of $Li_xAg_{1-x}Lu(MoO_4)_2$ matrices and the activator $Eu^{3+}$, another could be due to the near ultraviolet energy absorption and transmission efficiency between the charge-transfer (CT) band of $O^{2-}$–$Mo^{6+}$ and the 4f → 4f emissive transitions of $Eu^{3+}$. The ultraviolet-visible diffuse reflection spectra (UV-vis DRS) and Raman spectra analysis were also used to verify the above mechanism.

## 1. Introduction

Double molybdate scheelite-type compounds can be written as $M^{I}Ln^{III}(MoO_4)_2$. From the viewpoint of the structure and physical–chemical properties, most of these double molybdates are mainly classified into scheelite-type, wolframite-type, and pseudo-scheelite-type, respectively.[1,2] In the past few decades, $Eu^{3+}$-activated molybdates with scheelite-type structures have drawn much attention as potential red-emitting phosphor candidates for white light-emitting diodes (W-LEDs).[2–5] These materials usually have a broad and intense charge-transfer (CT) band in the UV region except for the intrinsic good stability and low synthetic temperature. The excitation intensity of $Eu^{3+}$ in molybdates at around 394 and 464 nm is significantly enhanced compared with that of $Eu^{3+}$ in other hosts.[6] Our previous work on the upconversion (UC) luminescence properties of molybdate $Li_xAg_{1-x}Yb_{0.99}(MoO_4)_2:0.01Er^{3+}$ phosphors verified that the variation of the nonradiative transition rates ($W_{NR}$) originating from the Li/Ag ratio played an important role in the enhancement of the UC emission.[7] Herein, new molybdates $Li_xAg_{1-x}Lu(MoO_4)_2:Eu^{3+}$ have been proposed, and we wonder whether such a host can also enhance the photoluminescence intensities of $Eu^{3+}$ depending on different chemical compositions, and it will give new insights into the modification of the luminescence properties of scheelite-type molybdate phosphors.

Recently, many reports have shown that the dopant of the alkali-metal $Li^+$ ion in the $Eu^{3+}$-activated molybdate materials can enhance the $Eu^{3+}$ emission intensity. For instance, Wang reported that the luminescence intensity of $CaMoO_4:Eu^{3+}/Li^+$ phosphor under excitation at 395 nm increased gradually with more $Eu^{3+}/Li^+$ substitution for $Ca^{2+}$, till the composition turned into $LiEuMo_2O_8$.[8] Liu discussed the dependence of the red emission intensity on the $Eu^{3+}$ concentration ($x$) in a range of molybdate phosphors under excitation at 393 nm.[9] Moreover, as for the phosphors $Ca_{1-2x}A_xMoO_4:xEu^{3+}$ (A = $K^+$, $Na^+$

[a]*School of Materials Sciences and Technology, China University of Geosciences, Beijing 100083, China*
[b]*School of Materials Sciences and Engineering, University of Science and Technology Beijing, Beijing 100083, China. E-mail: xiazg@ustb.edu.cn; Fax: +86-10-82377955; Tel: +86-10-82377955*
[c]*Laboratory of Crystal Physics, Kirensky Institute of Physics, SB RAS, Krasnoyarsk 660036, Russia*
[d]*Department of Physics, Far Eastern State Transport University, Khabarovsk, 680021 Russia*
[e]*Beijing National Laboratory for Molecular Sciences, State Key Laboratory of Rare Earth Materials Chemistry and Applications, College of Chemistry and Molecular Engineering, Peking University, Beijing 100871, China*

† Electronic supplementary information (ESI) available: XRD patterns of $LiLu_{1-x}Eu_x(MoO_4)_2$ ($x$ = 0.01, 0.05, 0.1, 0.2, 0.4, 0.6, 0.8, 1.0) and $AgLu_{1-x}Eu_x(MoO_4)_2$ ($x$ = 0.01, 0.1, 0.2, 0.4, 0.6, 0.8, 1.0), Li/Ag ratio dependent $I(^5D_0–^7F_1)/I(^5D_0–^7F_2)$ of $Li_xAg_{1-x}Lu_{0.95}(MoO_4)_2:0.05Eu^{3+}$, fractional atomic coordinates and isotropic displacement parameters (Å$^2$), main bond lengths (Å), and the crystallographic information files (CIF) of $AgEu(MoO_4)_2$, $AgLu(MoO_4)_2$, $LiLu(MoO_4)_2$ and $LiEu(MoO_4)_2$. See DOI: 10.1039/c5dt02760h


This journal is © The Royal Society of Chemistry 2015

Published on 16 September 2015. Downloaded by State Public Scientific Technical Library, Siberian Branch of the RAS on 10/19/2020 12:44:16 PM.

and $Li^+$), the emission intensity increases significantly with increasing contents of $Eu^{3+}$ and alkali-metal ions, and $Li^+$ ions have the best effect in this series. Therefore, the effect of alkali-metal $Li^+$ ions on the luminescence properties of $Eu^{3+}$-activated molybdates has been widely reported in the recent years.[10–15] It was found that the alkali-metal $Li^+$ ion could not only enhance the luminescence intensity and improve the color purity but also change the CT band of $O^{2-}$–$Mo^{6+}$ of the molybdate phosphors. However, the effects of alkali-metal $Li^+$ ions on the luminescence properties for molybdate host matrices are still not clear enough.

In this work, the crystal structures of $Li_{1-x}Ag_xLu_{1-y}(MoO_4)_2$:$yEu^{3+}$ solid-solution phosphors have been comparatively investigated, and four new phases of $AgEu(MoO_4)_2$, $AgLu(MoO_4)_2$, $LiLu(MoO_4)_2$ and $LiEu(MoO_4)_2$ have been firstly identified. It is found that the dopant of $Li^+$ ions can alter the spectral profiles of the excitation spectra of $Li_xAg_{1-x}Lu(MoO_4)_2$:$0.05Eu^{3+}$ phosphors, and the potential mechanism on the different luminescence properties has been analyzed based on the ultraviolet-visible diffuse reflection spectra (UV-vis DRS), and Raman spectra analysis.

## 2. Experimental section

### 2.1. Materials and synthesis

$Li_{1-x}Ag_xLu_{1-y}(MoO_4)_2$:$yEu^{3+}$ phosphors were synthesized by the high temperature solid-state reaction. $Li_2CO_3$ (A.R.), $AgNO_3$ (A.R.), $Mo_2O_3$ (A.R.), $Lu_2O_3$ (99.99%) and $Eu_2O_3$ (99.99%) were selected as the starting materials. The stoichiometric mixtures were mixed and ground thoroughly using a mortar, and the homogeneous mixtures were filled into porcelain crucibles respectively and then calcined in a muffle furnace at 750 °C for 12 h. The products obtained were found to be white or pink polycrystalline powder.

### 2.2. Characterization

The phase structures of the as-synthesized materials were determined by using a Rigaku D/max-rB X-ray diffractometer (Tokyo, Japan) with a Cu Kα (40 kV, 100 mA) incident source in the 5–120° $2\theta$ range (0.02°, $2\theta$ step size and 1 s per step). The crystallinity and morphology of the as-prepared phosphor samples were studied using a scanning electron microscope (SEM, Hitachi S-4800). The photoluminescence emission (PL) and excitation (PLE) spectra were recorded using a Hitachi F-7000 spectrometer with a 150 W Xe lamp as the excitation source under a working voltage of 400 V. The low-temperature PL spectra at 77 K were measured using the same FLS920 fluorescence spectrophotometer with a Xe900 lamp, and the sample temperature was varied using a temperature controller (Oxford, CRY TEMP). The decay curves were recorded on the same Edinburgh instrument (FLS920) with an nF900 flash lamp used as the excitation resource. The quantum efficiency (QE) was measured using an Absolute Photoluminescence Quantum Yield Measurement System (C9920-02, Hamamatsu-Photonics) with an integrating sphere at room temperature. The ultraviolet-visible diffuse reflection spectra (UV-vis DRS) were recorded on a UV–Vis–NIR spectrophotometer (UV-3600, Shimadzu). $BaSO_4$ served as a reference standard. The Raman spectra were recorded on a LabRAM Aramis micro-Raman spectrometer (HORIBA Jobin Yvon, France) with an excitation laser beam at 633 nm. The measurements were taken in backscattering configuration using a microscope with a 50× objective and a laser focal spot of ~1 $\mu m^2$.

## 3. Results and discussion

### 3.1. Phase analysis and crystal structure

Previous studies give some contradictory statements about the symmetry of the $LiEu(MoO_4)_2$ compound.[16–19] For example, Chiu *et al.*[16] proposed that $LiEu(MoO_4)_2$ is triclinic with the $P\bar{1}$ space group and with two molecular units per unit-cell, but Guo *et al.*[17] and Zaushutsyn *et al.*[18] suggested that $LiEu(MoO_4)_2$ belongs to the tetragonal crystal system with the space group $I4_1/a$ and showed that all peaks coincide with the peaks of tetragonal $AgEu(MoO_4)_2$ (PDF 53-0040) and tetragonal $LiEu(MoO_4)_2$ (PDF 52-1848). To solve this discrepancy, Chimitova *et al.*[19] made a collection of available structural parameters of $ALn(MoO_4)_2$ binary molybdates and suggested the relationship between the ionic radii ratio $t = R_{Ln}/R_A$ and the symmetry generated by different combinations of Ln and A atoms. Based on this, one can find that $LiEu(MoO_4)_2$ should have a $I4_1/a$ space group because it has $t = 0.863$ and all compounds with $t$ in the range 0.805–1.341 have a tetragonal unit cell with $I4_1/a$ or $I\bar{4}$ space groups and not a trigonal $P\bar{1}$ space group. In addition, the analysis of the crystal structure of $LiEu(MoO_4)_2$ with the $P\bar{1}$ space group showed some problems: (1) bond lengths Mo–O are in a very wide range of 1.8587(1)–2.3452(1) Å and the upper limit of this range is unusual for the Mo–O bond; (2) the volume of the primitive part of a unit cell is two times greater than the volume of the primitive cell of a hypothetical $I4_1/a$ cell but the superstructure peaks were not observed in the pattern; (3) $(Li/Eu)O_n$ polyhedra are very distorted. Thus, all of these facts allowed us to suggest that $LiEu(MoO_4)_2$ is in fact a tetragonal crystal system with a space group $I4_1/a$ .

Therefore, in order to give direct evidence on the phase formation and crystal structure of the $LiEu(MoO_4)_2$ structural evolution of the related $Li_{1-x}Ag_xLu_{1-y}(MoO_4)_2$:$yEu^{3+}$ phosphors is discussed in this paper. The four endpoint host compounds $AgEu(MoO_4)_2$, $AgLu(MoO_4)_2$, $LiLu(MoO_4)_2$ and $LiEu(MoO_4)_2$ of this series of solid-solutions $Li_{1-x}Ag_xLu_{1-y}(MoO_4)_2$:$yEu^{3+}$ were selected to reveal the detailed characteristics of the structure. Profile fitting and the following Rietveld refinements of the four compounds were performed by using TOPAS 4.2.[20] Almost all their peaks were indexed by a tetragonal cell ($I4_1/a$) with parameters close to $AgLa(MoO_4)_2$ based on the profile fitting results.[21] Therefore the crystal structure of $AgLa(MoO_4)_2$ was taken as the starting model for Rietveld refinement. The Rietveld plots for four samples are shown in Fig. 1a–d, respectively, and the main parameters of processing and refinement are

Published on 16 September 2015. Downloaded by State Public Scientific Technical Library, Siberian Branch of the RAS on 10/19/2020 12:44:16 PM.

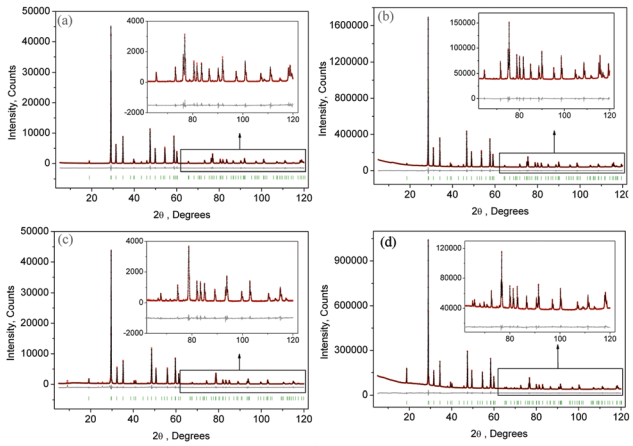


Fig. 1 Difference Rietveld plots of (a) $AgLu(MoO_4)_2$; (b) $AgEu(MoO_4)_2$; (c) $LiLu(MoO_4)_2$; (d) $LiEu(MoO_4)_2$.

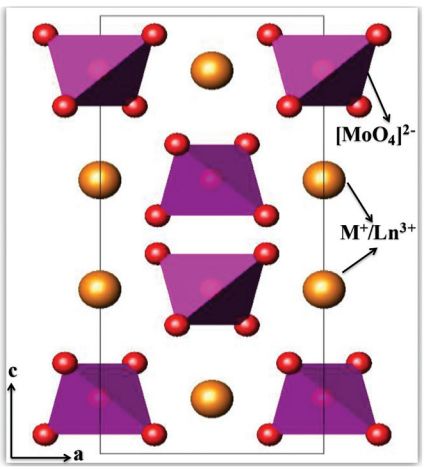


Fig. 2 The typical crystal structures of $MLn(MoO_4)_2$ (M = Ag, Li; Ln = Lu, Eu).

Table 1 Main parameters of processing and refinement of the selected $AgEu(MoO_4)_2$, $AgLu(MoO_4)_2$, $LiLu(MoO_4)_2$ and $LiEu(MoO_4)_2$ samples

| Compound | $AgLu(MoO_4)_2$ | $AgEu(MoO_4)_2$ | $LiLu(MoO_4)_2$ | $LiEu(MoO_4)_2$ |
|---|---|---|---|---|
| Sp. Gr. | $I4_1/a$ | $I4_1/a$ | $I4_1/a$ | $I4_1/a$ |
| $a$, Å | 5.17256(9) | 5.26334(2) | 5.10332(11) | 5.20263(2) |
| $c$, Å | 11.3926(2) | 11.5433(6) | 11.0829(3) | 11.33824(5) |
| $V$, Å$^3$ | 304.812(12) | 319.782(3) | 288.64(2) | 306.896(2) |
| $Z$ | 2 | 2 | 2 | 2 |
| $2\theta$-interval, ° | 5–120 | 5–120 | 5–120 | 5–120 |
| No. of reflections | 116 | 120 | 108 | 117 |
| No. of refined parameters | 8 | 8 | 8 | 8 |
| $R_{wp}$, % | 10.48 | 1.66 | 11.79 | 1.15 |
| $R_p$, % | 6.79 | 1.11 | 7.50 | 0.85 |
| $R_{exp}$, % | 5.71 | 0.43 | 4.82 | 0.42 |
| $\chi^2$ | 1.84 | 3.86 | 2.45 | 2.75 |
| $R_B$, % | 1.30 | 0.26 | 0.90 | 0.34 |

listed in Table 1. It is found that the refinement was stable and gives low $R$-factors (Table 1). The coordinates of atoms and main bond lengths are in Tables S1 and S2† respectively, which verified the structural occupancy of the different cations in this system. And the crystallographic information files (CIF) for $AgEu(MoO_4)_2$, $AgLu(MoO_4)_2$, $LiLu(MoO_4)_2$ and $LiEu(MoO_4)_2$ compounds are also given in ESI.† The above Rietveld refinement results suggest its real symmetry of $I4_1/a$ in all the studied compounds.

According to the crystallographic information, the crystal structures of $MLn(MoO_4)_2$ (M = Ag, Li; Ln = Lu, Eu) were well analysed. As for this kind of scheelite-type double molybdate shown in Fig. 2, the $Eu^{3+}$ and alkali metal $Li^+$ ions arbitrarily substitute for $Lu^{3+}$ and $Ag^+$ ions in the host lattice, respectively. Moreover, the positions of the $Lu^{3+}$ and $Ag^+$ ions are randomly distributed in the host of $AgLu(MoO_4)_2$. Hence, in the $MLn(MoO_4)_2$ (M = Ag, Li; Ln = Lu, Eu) crystal structures, the four oxygen atoms surround the $Mo^{6+}$ ions to form an isolated $[MoO_4]^{2-}$ tetrahedron, while the cations of $Li^+$, $Ag^+$, $Lu^{3+}$, $Eu^{3+}$ are arbitrarily distributed among the isolated $[MoO_4]^{2-}$ tetrahedra and replace each other, as also given in Fig. 2. Furthermore, since four endpoint components $AgEu(MoO_4)_2$, $AgLu(MoO_4)_2$, $LiLu(MoO_4)_2$ and $LiEu(MoO_4)_2$ share the same crystal structure, *i.e.*, tetragonal with the same space group of $I4_1/a$, the solid solution phase of these samples also maintained a tetragonal crystal structure. In this work, the components $AgLu(MoO_4)_2$ and $LiLu(MoO_4)_2$ were selected as matrices, and $Eu^{3+}$ acts as a good red emission activator ion.

The solid solutions of $AgLu_{1-x}Eu_x(MoO_4)_2$ ($x$ = 0.01, 0.1, 0.2, 0.4, 0.6, 0.8 and 1.0) and $LiLu_{1-x}Eu_x(MoO_4)_2$ ($x$ = 0.01, 0.05, 0.1, 0.2, 0.4, 0.6, 0.8 and 1.0) samples were prepared, and their XRD patterns are given in Fig. S1 and S2 in the ESI.† It was found that almost all the diffraction peaks of the products can be readily indexed to the pure tetragonal phase, and no impurity phase was found. Fig. 3 gives the linear dependence

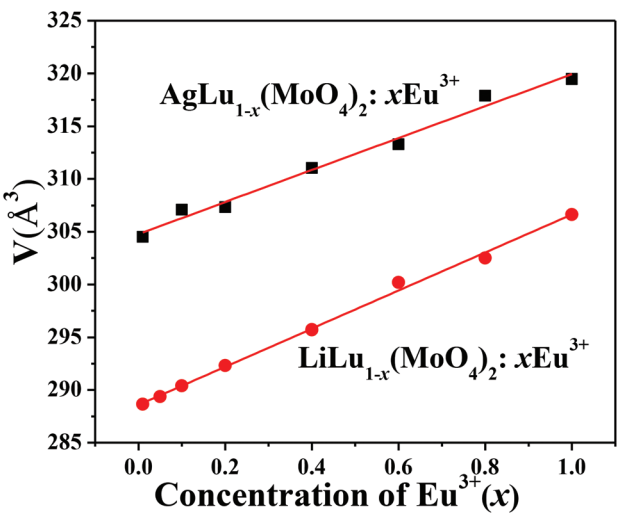


Fig. 3 Linear dependence of unit cell volume ($V$) as a function of $x$ values of $AgLu_{1-x}Eu_x(MoO_4)_2$ ($x$ = 0.01, 0.1, 0.2, 0.4, 0.6, 0.8 and 1.0) and $LiLu_{1-x}Eu_x(MoO_4)_2$ ($x$ = 0.01, 0.05, 0.1, 0.2, 0.4, 0.6, 0.8, 1.0).


This journal is © The Royal Society of Chemistry 2015

Published on 16 September 2015. Downloaded by State Public Scientific Technical Library, Siberian Branch of the RAS on 10/19/2020 12:44:16 PM.

of unit cell volume ($V$) as function of $x$ values in $AgLu_{1-x}Eu_x(MoO_4)_2$ ($x$ = 0.01, 0.1, 0.2, 0.4, 0.6, 0.8 and 1.0) and $LiLu_{1-x}Eu_x(MoO_4)_2$ ($x$ = 0.01, 0.05, 0.1, 0.2, 0.4, 0.6, 0.8, 1.0). As can be seen, the crystal structure remained the same though the Eu/Lu ratio in the host is different, which also indicates that $Lu^{3+}$ can be substituted for $Eu^{3+}$, forming a total range of continuous solid solutions of molybdates. There are evident shifts of the diffraction peaks depending on the different Eu/Lu ratios, as shown in the inset of Fig. S1 and S2.† This is attributed to the different ionic radii of $Eu^{3+}$ (1.066) and $Lu^{3+}$ (0.977) in the eight coordination, also implying that $AgLu_{1-x}Eu_x(MoO_4)_2$ ($x$ = 0.01, 0.1, 0.2, 0.4, 0.6, 0.8, 1.0) and $LiLu_{1-x}Eu_x(MoO_4)_2$ ($x$ = 0.01, 0.05, 0.1, 0.2, 0.4, 0.6, 0.8, 1.0) solid solutions are successfully synthesized and the lattice parameters can be modulated. Moreover, as $x$ values vary from 0 to 1.0, the volumes of the unit cell rise in linear dependence from 304.5 to 319.4 Å$^3$ in the $AgLu_{1-x}Eu_x(MoO_4)_2$ phosphors and from 288.6 to 306.6 Å$^3$ in the $LiLu_{1-x}Eu_x(MoO_4)_2$ phosphors, as shown in Fig. 3, which obey Vegard's law. The unit cell parameters of $AgLu_{1-x}Eu_x(MoO_4)_2$ ($x$ = 0.01, 0.1, 0.2, 0.4, 0.6, 0.8, 1.0) and $LiLu_{1-x}Eu_x(MoO_4)_2$ ($x$ = 0.01, 0.05, 0.1, 0.2, 0.4, 0.6, 0.8, 1.0) solid solutions are also shown in Tables 2 and 3, respectively. These results attest that the crystalline structure achieves continuous variation and retains the same tetragonality though the $x$ values vary from 0 to 1.0.

Except for the variation of the Eu/Lu ratio, the crystalline structure of $MLn(MoO_4)_2$ (M = Ag, Li; Ln = Lu, Eu) series can also remain unchanged depending on the Ag/Li ratio. Thus, $Li_xAg_{1-x}Lu_{0.95}(MoO_4)_2$:$0.05Eu^{3+}$ ($x$ = 0, 0.2, 0.4, 0.6, 0.8, 1.0) were chosen as typical phosphors suggesting the influence of different Ag/Li ratios on the structure and luminescence properties. $AgLu(MoO_4)_2$ and $LiLu(MoO_4)_2$ share the same tetragonal crystal structure with the same space group of $I4_1/a$, as shown in Fig. 1. Based on the different Li/Ag ratios in the $Li_xAg_{1-x}Lu(MoO_4)_2$ host, the crystal structure remained because of the similar characteristics of $Ag^+$ and $Li^+$, as given in the XRD patterns in Fig. 4(a). It also shows that $Ag^+$ can be replaced with $Li^+$, forming a full-range of continuous solid solutions of molybdates. There are also obvious shifts of the diffraction peaks due to the different Li/Ag ratios as shown in the inset of Fig. 4(a), since the ionic radii of $Li^+$ (0.92 Å) and $Ag^+$ (1.28 Å) are different in the eight coordination, also meaning that $Li_xAg_{1-x}Lu_{0.95}(MoO_4)_2$:$0.05Eu^{3+}$ solid-solution phosphors were successfully synthesized and the cell parameters can be well modulated. In addition, the tetragonality ($c/2a$) of this series of $Li_xAg_{1-x}Lu_{0.95}(MoO_4)_2$:$0.05Eu^{3+}$ samples as a function of $x$ is plotted as shown in Fig. 4(b). Due to the different ionic radii of $Li^+$ (0.92) and $Ag^+$ (1.28) in the eight coordination, the tetragonality $c/2a$ ratio declines in linear dependence from 1.10041 to 1.08594 as $x$ values vary from 0 to

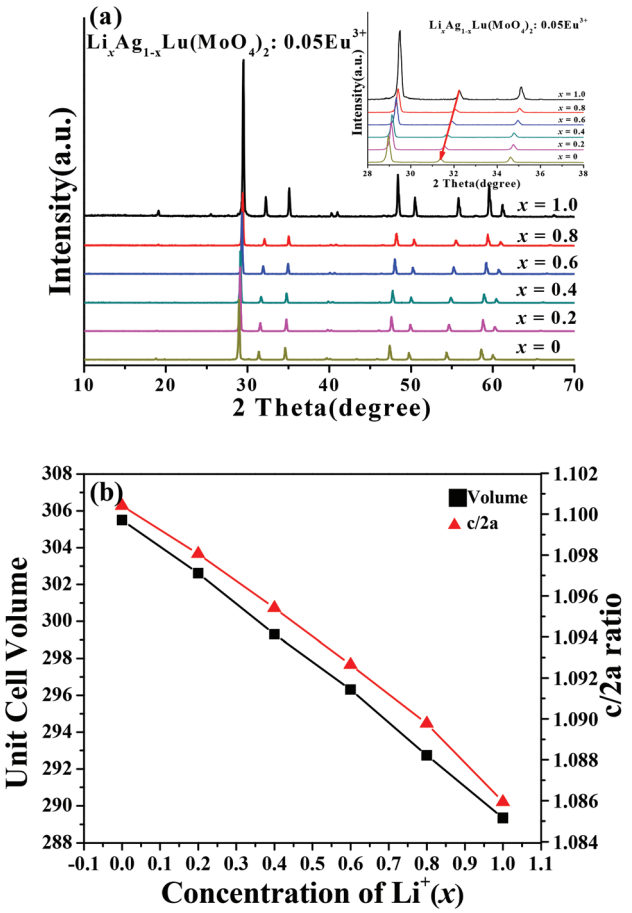


Fig. 4 XRD patterns (a) and linear dependence of $c/2a$ ratio and unit cell volume ($V$) as function of $x$ values (b) of $Li_xAg_{1-x}Lu_{0.95}(MoO_4)_2$:$0.05Eu^{3+}$ ($x$ = 0, 0.2, 0.4, 0.6, 0.8 and 1.0).

Table 2 The unit cell parameters of $AgLu_{1-x}Eu_x(MoO_4)_2$ ($x$ = 0.01, 0.1, 0.2, 0.4, 0.6, 0.8, 1.0)

| $x$ | $a$ | $c$ | $V$/Å$^3$ |
|---|---|---|---|
| 0.01 | 5.1720(7) | 11.3841(7) | 304.5(3) |
| 0.1 | 5.1892(9) | 11.4042(9) | 307.1(0) |
| 0.2 | 5.1905(3) | 11.4072(1) | 307.3(3) |
| 0.4 | 5.2141(1) | 11.4402(7) | 311.0(3) |
| 0.6 | 5.2258(2) | 11.4720(3) | 313.2(9) |
| 0.8 | 5.2555(9) | 11.5088(0) | 317.8(9) |
| 1 | 5.2610(1) | 11.5418(4) | 319.4(6) |

Table 3 The unit cell parameters of $LiLu_{1-x}Eu_x(MoO_4)_2$ ($x$ = 0.01, 0.05, 0.1, 0.2, 0.4, 0.6, 0.8, 1.0)

| $x$ | $a$ | $c$ | $V$/Å$^3$ |
|---|---|---|---|
| 0.01 | 5.1039(5) | 11.0802(0) | 288.6(4) |
| 0.05 | 5.1073(4) | 11.0935(6) | 289.3(7) |
| 0.1 | 5.1129(5) | 11.1084(2) | 290.4(0) |
| 0.2 | 5.1236(4) | 11.1355(8) | 292.3(3) |
| 0.4 | 5.1426(1) | 11.1817(4) | 295.7(2) |
| 0.6 | 5.1649(0) | 11.2532(9) | 300.1(9) |
| 0.8 | 5.1790(1) | 11.2780(3) | 302.5(0) |
| 1 | 5.2006(0) | 11.3378(1) | 306.6(4) |

Published on 16 September 2015. Downloaded by State Public Scientific Technical Library, Siberian Branch of the RAS on 10/19/2020 12:44:16 PM.

Table 4 The unit cell parameters of $Li_xAg_{1-x}Lu_{0.95}(MoO_4)_2$:0.05$Eu^{3+}$ ($x$ = 0, 0.2, 0.4, 0.6, 0.8, 1.0)

| $x$ | $a$ | $c$ | $V$/Å$^3$ |
|---|---|---|---|
| 0 | 5.177(8) | 11.395(3) | 305.5(1) |
| 0.2 | 5.165(1) | 11.343(2) | 302.6(2) |
| 0.4 | 5.150(3) | 11.283(4) | 299.3(2) |
| 0.6 | 5.137(4) | 11.226(8) | 296.3(1) |
| 0.8 | 5.121(2) | 11.161(9) | 292.7(4) |
| 1 | 5.107(3) | 11.092(3) | 289.3(4) |

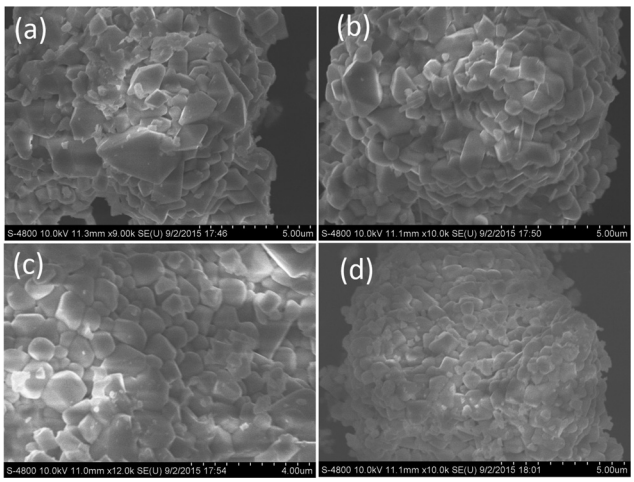


Fig. 5 SEM images of selected $Li_{1-x}Ag_xLu_{0.95}(MoO_4)_2$:0.05$Eu^{3+}$ phosphors, a: $x$ = 0, b: $x$ = 0.2, c: $x$ = 0.5 and d: $x$ = 1.

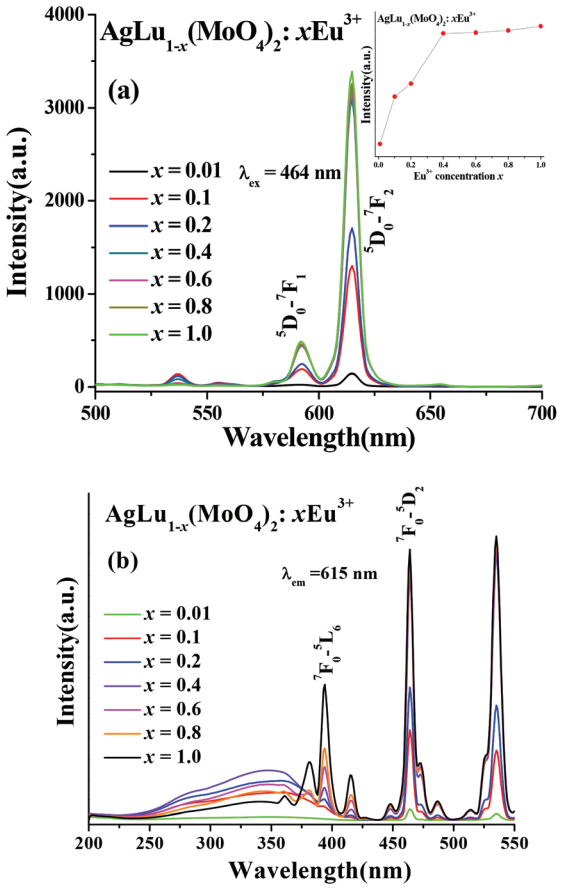


Fig. 6 The PL (a) ($\lambda_{ex}$ = 464 nm) and PLE (b) ($\lambda_{em}$ = 615 nm) spectra of $AgLu_{1-x}Eu_x(MoO_4)_2$ ($x$ = 0.01, 0.1, 0.2, 0.4, 0.6, 0.8 and 1.0) phosphors, and the inset of (a) shows the dependence of PL intensities on the $Eu^{3+}$ doping concentration.

1.0, and the volume of the unit cell also reduces in linear dependence from 305.5 to 289.3 Å$^3$, which also obey Vegard's law. The results are also shown in Table 4.

Fig. 5 shows the SEM images of the selected $Li_{1-x}Ag_xLu_{0.95}(MoO_4)_2$:0.05$Eu^{3+}$ ($x$ = 0, 0.2, 0.5 and 1.0) phosphors. From the SEM images, we can find some irregular rectangle particles with the diameters of 1–2 μm, and the morphology and size don't change a lot depending on the different Li/Ag ratios. Hence we can assume that the observed variation of spectral profiles is mainly due to the changes of covalent properties of the Li/Ag compounds, not the crystallinity and morphology of the as-prepared phosphors.

### 3.2. Luminescence properties of $Eu^{3+}$ doped $MLu(MoO_4)_2$ phosphors

Fig. 6(a) shows the PL spectra of $AgLu_{1-x}Eu_x(MoO_4)_2$ ($x$ = 0.01, 0.1, 0.2, 0.4, 0.6 and 0.8, 1.0) phosphors under the excitation of 464 nm blue light. All the emission spectra consist of a group of sharp lines with wavelengths ranging from 500 nm to 700 nm, which are assigned to the $^5D_0 \rightarrow {}^7F_J$ ($J$ = 1, 2, 3) multiplet transitions from the excited levels of $Eu^{3+}$ to the ground state. Among all emission lines of each phosphor, the shapes of emission spectra are similar. And the strongest red emission lines peaked at 615 nm due to the electric dipole transition $^5D_0 \rightarrow {}^7F_2$, suggesting that the $Eu^{3+}$ occupies the lattice site of the noncentrosymmetric environment in the present phases, while another group of relatively weak orange emission lines at 593 nm are due to the magnetic dipole transitions of $^5D_0 \rightarrow {}^7F_1$. Other transitions from the $^5D_J$ excited levels to $^7F_J$ ground states of $Eu^{3+}$, for instance, both $^5D_0 \rightarrow {}^7F_3$ transition located at 650–700 nm and the $^5D_1 \rightarrow {}^7F_J$ transition located at 500–570 nm are very weak. Moreover, as shown in Fig. 6(a), with an increasing $Eu^{3+}$ content, the luminescence intensity of $AgLu_{1-x}Eu_x(MoO_4)_2$ ($x$ = 0.01, 0.1, 0.2, 0.4, 0.6, 0.8, 1.0) red phosphors increased gradually. When the $Eu^{3+}$ content is 1.0, the luminescence intensity is saturated, and the $Eu^{3+}$ has no quenching concentration in the $AgLu(MoO_4)_2$ host. Being monitored at 615 nm attributed to the $^5D_0 \rightarrow {}^7F_2$ emission of $Eu^{3+}$ ions, the PLE spectra of the selected compositions of $AgLu_{1-x}Eu_x(MoO_4)_2$ ($x$ = 0.01, 0.1, 0.2, 0.4, 0.6, 0.8, 1.0) are shown in Fig. 6(b). The PLE spectra consist of two parts, one is composed of the broad band ranging from 200 to ~400 nm, which is assigned as the charge-transfer (CT) transition originating from oxygen to molybdenum and europium (*i.e.*, ligand to metal CT).[22,23] Compared to the CT band of


This journal is © The Royal Society of Chemistry 2015

Published on 16 September 2015. Downloaded by State Public Scientific Technical Library, Siberian Branch of the RAS on 10/19/2020 12:44:16 PM.

$O^{2-}$–$Mo^{6+}$, the CT band of $O^{2-}$–$Eu^{3+}$ is located in the short ultraviolet wavelength region (250–320 nm) in the double molybdate phosphors, therefore, the long wavelength region of the broad band is mainly ascribed to the CT band of $O^{2-}$–$Mo^{6+}$ as shown in Fig. 6(b). It is also found that the observed CT band is obviously different from the CT band of $Eu^{3+}$ in the $ZnWO_4$ and $CdWO_4$ hosts.[24,25] With the increase of the $Eu^{3+}$ concentration in the matrix, the long wavelength region of the broad band is shifting, the CT band of $O^{2-}$–$Mo^{6+}$ move to the left, that is to say, the near ultraviolet light absorption range of the $AgLu_{1-x}Eu_x(MoO_4)_2$ phosphors tends to become narrow. This phenomenon suggests energy transfer appearing between the CT band of $O^{2-}$–$Mo^{6+}$ in the $[MoO_4]^{2-}$ and the luminescence center $Eu^{3+}$ through the oxygen ligand.[2,26] Another part in the PLE spectra contains a series of sharp peaks ranging from ~400 to 550 nm, which is ascribed to the characteristic intra-configurational 4f → 4f emissive transitions of $Eu^{3+}$: sharp $^7F_0 \rightarrow {}^5L_6$ transition at 394 nm, $^7F_0 \rightarrow {}^5D_2$ transition at 464 nm, and the $^7F_1 \rightarrow {}^5D_1$ transition at 534 nm. However, parts of sharp line transitions were not clearly observed in the excitation spectra, which could be due to the overlap of the CT band with that of the molybdate group. With increasing $Eu^{3+}$ concentrations, the intensities of the sharp peak intensity of $AgLu_{1-x}Eu_x(MoO_4)_2$ ($x$ = 0.01, 0.1, 0.2, 0.4, 0.6, 0.8, 1.0) phosphors are enhanced, which is consistent with the PL intensity shown in Fig. 6(a).

Similarly, Fig. 7(a) shows the PL spectra of $LiLu_{1-x}(MoO_4)_2$: $xEu^{3+}$ ($x$ = 0.01, 0.05, 0.1, 0.2, 0.4, 0.6, 0.8, 1.0) phosphors under the excitation at 396 nm near ultraviolet light. It is found that the strongest red emission line is peaked at 618 nm and the optimum $Eu^{3+}$ content is 0.8. Being monitored at 618 nm, the PLE spectra of this series of samples are shown in Fig. 7(b). The PLE spectra also consist of two parts, one is corresponding to the broad band ranging from 200 to 360 nm, and another part contains a series of sharp peaks ranging from 360 to 550 nm, which is the same as the result shown in the above Fig. 6. With increasing $Eu^{3+}$ concentrations, the broad absorption band becomes much stronger, which is due to the effect of the CT band of $O^{2-}$–$Mo^{6+}$ and $O^{2-}$–$Eu^{3+}$. We also think that this should be related to the energy transfer between the CT band of $O^{2-}$–$Mo^{6+}$ and the luminescence center $Eu^{3+}$.

By comparing the results shown in Fig. 6 and 7, the spectral profiles of the PLE spectra of $AgLu_{1-x}Eu_x(MoO_4)_2$ and $LiLu_{1-x}Eu_x(MoO_4)_2$ phosphors are quite different. The near ultraviolet light absorption range of $AgLu_{1-x}Eu_x(MoO_4)_2$ phosphors is much greater than that of $LiLu_{1-x}Eu_x(MoO_4)_2$ phosphors. However, the near ultraviolet energy absorption and transmission efficiency of the $LiLu_{1-x}Eu_x(MoO_4)_2$ phosphors are higher than that of the $AgLu_{1-x}Eu_x(MoO_4)_2$ phosphors. As we know, continuous solid solutions can be obtained from the $MLn(MoO_4)_2$ (M = Ag, Li; Ln = Lu, Eu) compounds, and the luminescence intensities of $AgLu_{1-x}Eu_x(MoO_4)_2$ and $LiLu_{1-x}Eu_x(MoO_4)_2$ phosphors both tend to be saturated with increasing $Eu^{3+}$ concentrations. Thus, $Li_xAg_{1-x}Lu_{0.95}(MoO_4)_2$:$0.05Eu^{3+}$ was selected by changing the Ag/Li ratio, in order to study the

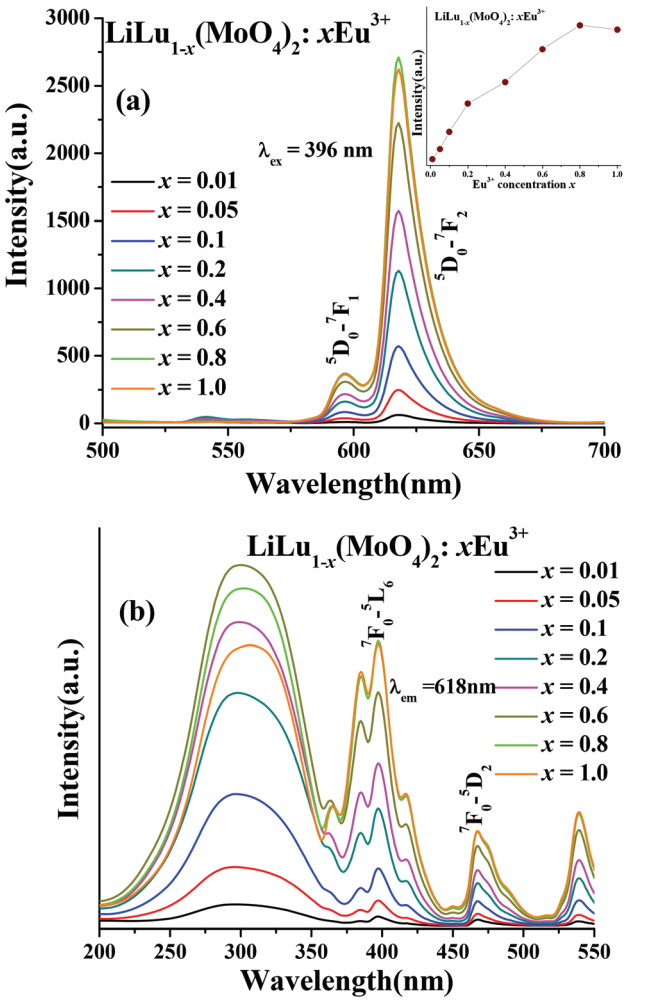


Fig. 7 The PL (a) ($\lambda_{ex}$ = 396 nm) and PLE spectra (b) ($\lambda_{em}$ = 618 nm) of $LiLu_{1-x}Eu_x(MoO_4)_2$ ($x$ = 0.01, 0.05, 0.1, 0.2, 0.4, 0.6, 0.8 and 1.0) phosphors, and the inset shows the dependence of PL intensities on the $Eu^{3+}$ doping concentration.

effect of Ag/Li ratio composition modulation on the luminescence properties.

Fig. 8(a) and (b) show the PL spectra of $Li_xAg_{1-x}Lu_{0.95}(MoO_4)_2$:$0.05Eu^{3+}$ ($x$ = 0, 0.2, 0.4, 0.6, 0.8, 1.0) phosphors under different excitation wavelengths of 394 nm and 464 nm. The strongest red emission line all peaked at 615 nm suggesting that the Ag/Li ratio does not change the noncentrosymmetric environment of the luminescence center $Eu^{3+}$ in the present system. As shown in Fig. 8(a), the luminescence intensities of $Li_xAg_{1-x}Lu_{0.95}(MoO_4)_2$:$0.05Eu^{3+}$ phosphors is enhanced with increasing $Li^+$ concentrations under excitation wavelength of 394 nm, and the $LiLu_{0.95}(MoO_4)_2$:$0.05Eu^{3+}$ phosphor has the strongest luminescence intensity. As shown in Fig. 8(b), under excitation at 464 nm, the luminescence intensities of $Li_xAg_{1-x}Lu_{0.95}(MoO_4)_2$:$0.05Eu^{3+}$ are also enhanced with increasing $Li^+$ concentrations, and the $Li_{0.8}Ag_{0.2}Lu_{0.95}(MoO_4)_2$:$0.05Eu^{3+}$ phosphor has the strongest luminescence

Published on 16 September 2015. Downloaded by State Public Scientific Technical Library, Siberian Branch of the RAS on 10/19/2020 12:44:16 PM.

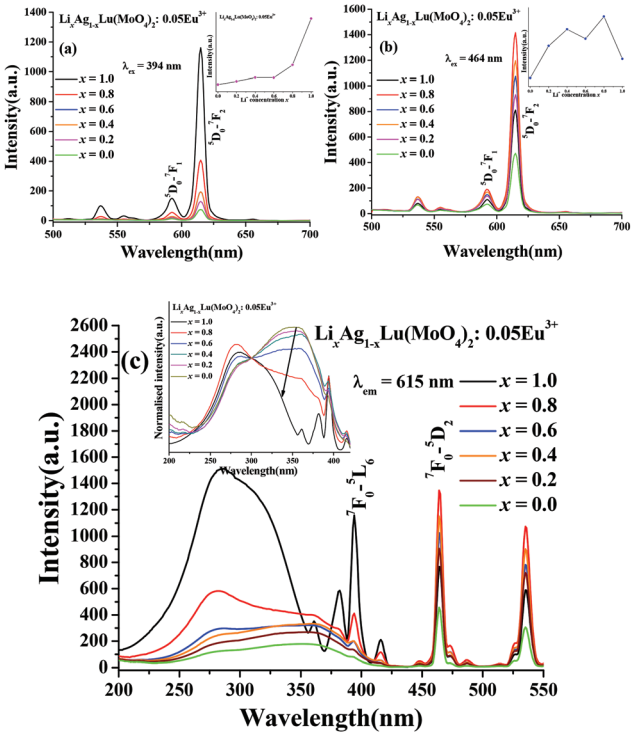


Fig. 8 PL spectra (a: $\lambda_{ex}$ = 394 nm; b: $\lambda_{ex}$ = 464 nm) and PLE spectra (c: $\lambda_{em}$ = 615 nm) of $Li_xAg_{1-x}Lu(MoO_4)_2$:0.05$Eu^{3+}$ ($x$ = 0, 0.2, 0.4, 0.6, 0.8 and 1.0) phosphors, and the insets in (a) and (b) show the dependence of PL intensity on the $Li^+$ doping concentration; and the inset in (c) shows the normalized excitation spectra in the range of 200–420 nm.

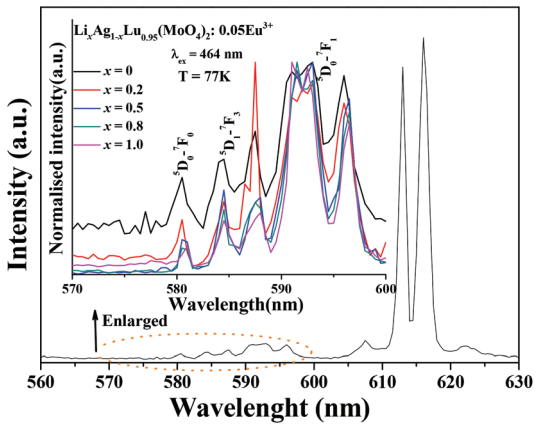


Fig. 9 PL spectrum at 77 K of $AgLu_{0.95}(MoO_4)_2$:0.05$Eu^{3+}$, and the inset shows the comparison of the PL spectra at 77 K of $Li_xAg_{1-x}Lu_{0.95}(MoO_4)_2$:0.05$Eu^{3+}$ ($x$ = 0, 0.2, 0.5, 0.8, 1.0) phosphors in the range of 570–600 nm.

intensity. The absolute quantum efficiency (QE) of the selected $LiEu(MoO_4)_2$ is about 24% under excitation at 460 nm.

Fig. 8(c) shows the PLE spectra of five samples with selected compositions of $Li_xAg_{1-x}Lu_{0.95}(MoO_4)_2$:0.05$Eu^{3+}$ ($x$ = 0, 0.2, 0.4, 0.6, 0.8, 1.0) phosphors monitored at 615 nm. With the increase of $Li^+$ concentrations in the matrix, the CT band of $O^{2-}$–$Mo^{6+}$ of the broad band is shifting to the left, the near ultraviolet light absorption range of $Li_xAg_{1-x}Lu_{0.95}(MoO_4)_2$:0.05$Eu^{3+}$ ($x$ = 0, 0.2, 0.4, 0.6, 0.8, 1.0) phosphors becomes much narrower but the near ultraviolet energy absorption and transmission efficiency becomes greater. As a comparison, the broad absorption band is becoming much stronger. As given in the inset of Fig. 8(c), such a variation can be clearly found from the normalized excitation spectra. That's to say, the luminescence intensities of the molybdate phosphors are not only related to the coupling nonradiative transition probabilities of the phonons but also associated with near ultraviolet energy absorption and transmission efficiency between the CT band of $O^{2-}$–$Mo^{6+}$ and the 4f → 4f emissive transitions of $Eu^{3+}$.

In order to improve the spectral resolution and better understand the local symmetry/environments at $Eu^{3+}$ sites, the low temperature measurement of the PL spectra is essential and some interesting results can be demonstrated.[27,28] Fig. 9 gives the PL spectrum at 77 K of $AgLu_{0.95}(MoO_4)_2$:0.05$Eu^{3+}$ and the comparison of PL spectra at 77 K of $Li_xAg_{1-x}Lu_{0.95}(MoO_4)_2$:0.05$Eu^{3+}$ ($x$ = 0, 0.2, 0.5, 0.8, 1.0) phosphors in the range of 570–600 nm. It is found that $^5D_0$–$^7F_2$ (615 nm) transition is obviously dominating showing the strong red emission, moreover, from the enlarged high resolution spectra, $^5D_0$–$^7F_0$ transition around 579 nm has one peak and $^5D_0$–$^7F_1$ transition from 590 nm to 600 nm has two peaks. $^5D_0$–$^7F_0$ transition around 579 nm has one peak which means that Eu only has one site depending on the evolution of the Li/Ag ratio. Moreover, the number of peaks for $^5D_0$–$^7F_1$ transition allows us to make a crude separation and prediction of the point group.[29] Two peaks are an indication of hexagonal, trigonal or tetragonal point groups, which is the same as the above-mentioned crystal structure analysis (tetragonal unit cell in the present case). We have also calculated the intensity ratios of $^5D_0$–$^7F_1$ (at 590 nm) and $^5D_0$–$^7F_2$ (615 nm) transitions from the room temperature $Eu^{3+}$ ion emission spectrum ($\lambda_{ex}$ = 464 nm) in Fig. 8, and the variation of the intensity ratios is given in Fig. S3 in the ESI.† We can clearly find that ratios remain nearly unchanged (about 0.2) and this value at 77 K will be smaller than that at room temperature suggesting $Eu^{3+}$ occupied a low symmetry.

Furthermore, the decay curves of $Li_{1-x}Ag_xLu_{0.95}(MoO_4)_2$:0.05$Eu^{3+}$ ($x$ = 0, 0.2, 0.5, 0.8, 1.0) phosphors at room temperature were measured by monitoring the $^5D_0$–$^7F_2$ (615 nm) transitions under excitation at 394 nm and 464 nm, respectively. It can be clearly found that all the decay curves obey the single exponential decay fitting, which verified that all $Eu^{3+}$ ions occupy the same crystal environment in this series of samples. Moreover, the lifetime values remain nearly unchanged (about 0.36 ms), however, the lifetime value of Ag-rich samples is about 0.1 ms shorter than that of Li-rich samples. This should be due to the Ag-rich samples having a lower band gap, and the energy of $Eu^{3+}$ being much closer to the Mo–O CT than that of Li-rich samples, and then the

 This journal is © The Royal Society of Chemistry 2015

Published on 16 September 2015. Downloaded by State Public Scientific Technical Library, Siberian Branch of the RAS on 10/19/2020 12:44:16 PM.

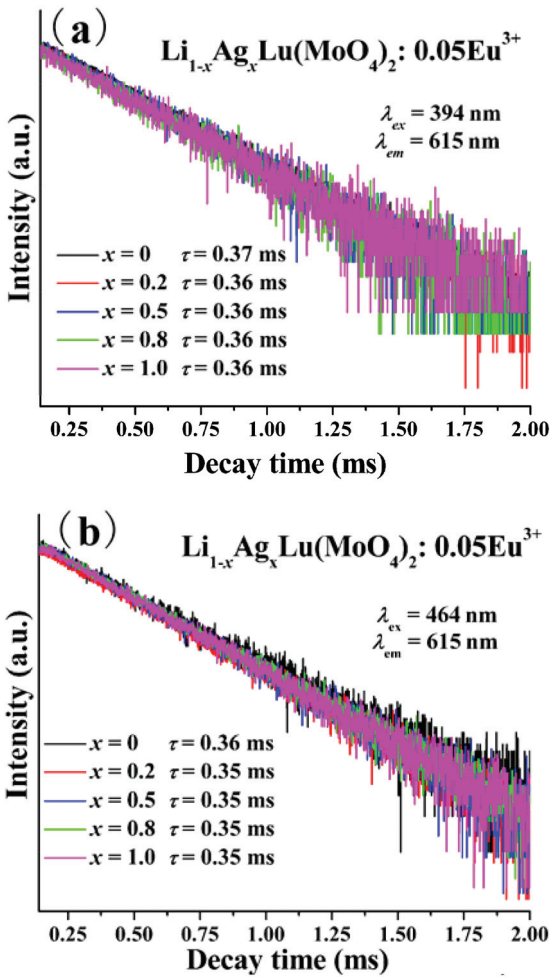


**Fig. 10** Decay curves of $Li_{1-x}Ag_xLu_{0.95}(MoO_4)_2$:0.05$Eu^{3+}$ ($x$ = 0, 0.2, 0.5, 0.8, 1.0) at room temperature: (a) monitoring at 615 nm under excitation at 394 nm; (b) monitoring at 615 nm under excitation at 464 nm.

electron in the excited state may gain an extra quenching way resulting in a short decay behavior (Fig. 10).

### 3.3. Relationship between the $Eu^{3+}$ energy level and the host in $MLu(MoO_4)_2$:$Eu^{3+}$ phosphors

In order to further discuss the mechanism on the effect of Ag/Li ratio composition modulation on the luminescence properties, the UV-vis DRS of phosphors $Li_xAg_{1-x}Lu_yEu_{1-y}(MoO_4)_2$ ($x$ = 0, 1.0; y = 0, 0.6, 1.0) and undoped hosts $Li_xAg_{1-x}Lu(MoO_4)_2$ ($x$ = 0, 1.0) were measured and calculated, respectively, and the relationship between the absorption coefficient and the photon energy is shown in Fig. 11. As shown in Fig. 11, it is found that the obvious difference of the band gaps ($E_g$) is not ascribed to the substitution of $Lu^{3+}$ for $Eu^{3+}$, but the result of $Li^+$ substitution for $Ag^+$. As can be seen from Fig. 11, the band gaps of $Li_xAg_{1-x}Lu(MoO_4)_2$ ($x$ = 0, 1.0) are obviously different, which should be due to the different electronegativity values of $Li^+$ (0.91) and $Ag^+$ (1.87).[30] Therefore, it will lead to the different covalent properties of the host crystal lattice. On the basis of Pankove's and Hao's suggestion,[31,32] the reflection spectrum was expressed as the following eqn (1):

$$(\alpha h\nu)^2 \propto h\nu \quad (1)$$

where $\alpha$ represented the reflection coefficient, $h$ is the Planck's constant, and $\nu$ is the frequency of light. Therefore, the band gap value ($E_g$) was measured from the low energy edge (the long wavelength edge) of the absorption band in the reflection spectrum. The $E_g$ values of $Li_xAg_{1-x}Lu(MoO_4)_2$ ($x$ = 0, 1.0) were determined to be 3.08 eV, and 3.58 eV, respectively. Thus, as shown in Fig. 11, the increasing $E_g$ value was expected to enhance the $Eu^{3+}$ emission due to the decrease of covalent properties of the host lattice. To find out the difference between $Eu^{3+}$ emission and excitation intensities in this series of $Li_xAg_{1-x}Lu(MoO_4)_2$, their relationships among the ionic polarizations, deformation abilities of the ions and band gap have also been introduced.[7] At the same time, the relationship between the band gap value ($E_g$) and $Eu^{3+}$ luminescence intensity has been well studied, as shown in Fig. 12. It is commonly recognized that the band gap is closely related to the polarization ability of cations and the deformation ability of ions. Particularly, the polarization ability of cations has been taken into account. The greater the cationic polarization ability is, the stronger the covalent bond links to the anion, which in turn results in the narrower band gap. In order to give a further comprehension of the increasing $E_g$ value extension with the increasing $x$ values of the $Li_xAg_{1-x}Lu_{0.95}(MoO_4)_2$:0.05$Eu^{3+}$ ($x$ = 0, 0.2, 0.5, 0.8, 1.0) phosphors, the following expression has been proposed, as given in eqn (2):

$$\phi_{\text{eff}} = Z_{\text{eff}}/r \quad (2)$$

The effective ionic potential ($\Phi_{\text{eff}}$) is introduced to measure the polarization ability of cations (Fig. 12). The function $Z_{\text{eff}}$ is called the effective cationic nuclear charge, and $r$ is the cationic radius in the corresponding ligand field.[33] Based on this equation, the effective cationic nuclear charge results of $Ag^+$ and $Li^+$ are $\Phi_{Ag^+}$ = 3.63 and $\Phi_{Li^+}$ = 1.41, respectively, which indicate that the polarization ability of $Ag^+$ is much greater than that of $Li^+$. As shown in Fig. 12, oxygen ions have more deformation in the $AgLu_{0.95}(MoO_4)_2$:0.05$Eu^{3+}$ system compared to that of the $LiLu_{0.95}(MoO_4)_2$:0.05$Eu^{3+}$ system, which will lead to

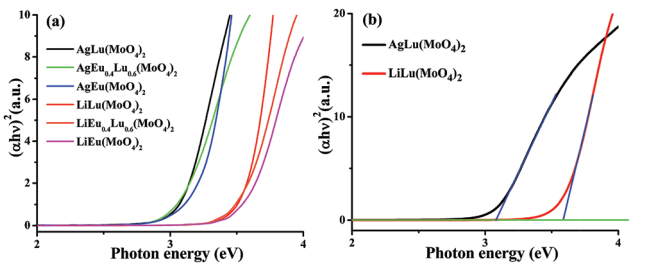


**Fig. 11** The relationship between the absorption coefficient and the photon energy for (a) $Li_xAg_{1-x}Lu_yEu_{1-y}(MoO_4)_2$ ($x$ = 0, 1.0; $y$ = 0, 0.6, 1.0); and (b) $Li_xAg_{1-x}Lu(MoO_4)_2$ ($x$ = 0, 1.0).

Published on 16 September 2015. Downloaded by State Public Scientific Technical Library, Siberian Branch of the RAS on 10/19/2020 12:44:16 PM.

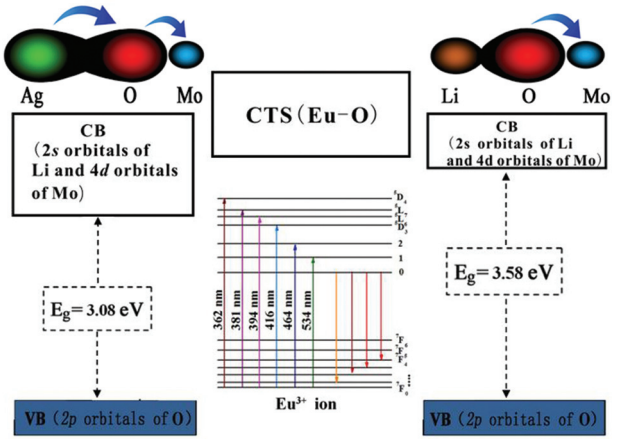


Fig. 12 Electron cloud polarizations and ionic deformations of $AgLu_{0.95}(MoO_4)_2$:0.05$Eu^{3+}$ and $LiLu_{0.95}(MoO_4)_2$:0.05$Eu^{3+}$; energy level diagrams of $ALu_{0.95}(MoO_4)_2$:0.05$Eu^{3+}$ (A = Li or Ag).

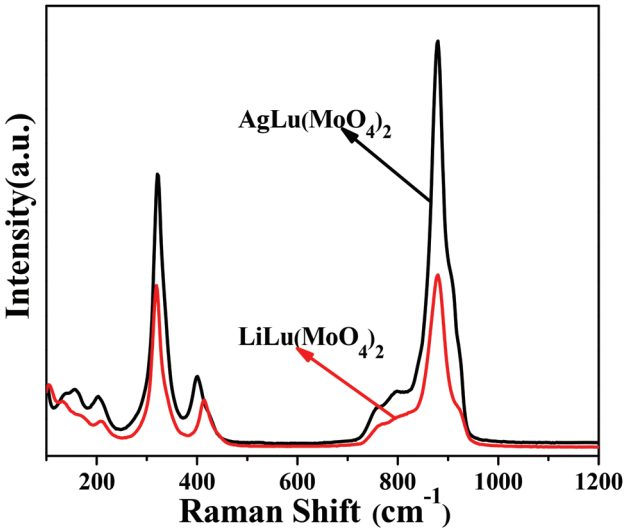


Fig. 13 Raman spectra of undoped $AgLu(MoO_4)_2$ and $LiLu(MoO_4)_2$ host materials excited at 633 nm.

the enhancement of covalent properties of the Ag–O bond. Hence, in the $Li_xAg_{1-x}Lu_{0.95}(MoO_4)_2$:0.05$Eu^{3+}$ ($x$ = 0, 0.2, 0.5, 0.8, 1.0) phosphors, when $Ag^+$ is replaced with $Li^+$, the band gaps of the $Li_xAg_{1-x}Lu(MoO_4)_2$ host become wider. Besides, the deformation ability of ions should be also considered. Since the $Li_xAg_{1-x}Lu_{0.95}(MoO_4)_2$:0.05$Eu^{3+}$ ($x$ = 0, 0.2, 0.5, 0.8, 1.0) phosphors share the same Mo–O bond, the difference between the deformation abilities of $Li^+$ and $Ag^+$ is primarily discussed. Based on the theory on Lewis hard and soft acids and bases,[33] $Li^+$ is difficult to be deformed since it possesses a two electron configuration and only 1s orbital having two electrons with small ionic radius and high charge density. Therefore, $Li^+$ belongs to the hard acid. While $Ag^+$ has the eighteen electron configuration and its outer shell layer contains $4d^{10}$ orbital with large ionic radius and low charge density, $Ag^+$ is easy to deform and it is called the soft acid. Hence, based on the above analysis, the arrows show the moving direction of the electron cloud, as shown in Fig. 12, which is also regarded as the effect of electron cloud expansion,[34] and the deformation ability of $Ag^+$ is greater than that of $Li^+$, which will generate the phenomenon that the $Ag^+$ feeds back much more electron cloud to the Mo–O bond in the $AgLu_{0.95}(MoO_4)_2$:0.05$Eu^{3+}$ system than that of $Li^+$ in the $LiLu_{0.95}(MoO_4)_2$:0.05$Eu^{3+}$ system. Thus the covalent properties of the Mo–O bond in the $AgLu_{0.95}(MoO_4)_2$:0.05$Eu^{3+}$ system is much greater than that of the $LiLu_{0.95}(MoO_4)_2$:0.05$Eu^{3+}$ system.

Fig. 13 gives the Raman spectra of $AgLu(MoO_4)_2$ and $LiLu(MoO_4)_2$ hosts under the excitation of 633 nm laser, and the result indicates that the maximum phonon energy of $AgLu(MoO_4)_2$ and $LiLu(MoO_4)_2$ host materials is almost the same. As we can also observe from Fig. 13 that the Raman spectra of the bands at 318, 403, 790, and 880 $cm^{-1}$ can be divided into two groups, which show the clear multiplets of the stretching $\nu$(Mo–O) vibrations in the range of 750–1000 $cm^{-1}$ and the bending vibrations in the range of 300–450 $cm^{-1}$.[35] Moreover, the theory on lattice relaxation and multiphonon transitions has been well established.[36–39] In the case of rare-earth luminescence centers, the coupling between centers and the lattice is relatively weak because the 4f electrons are shielded by 5s and 5p electrons.[40] If the doped concentrations of rare earth ions and the maximum phonon energy remain the same, the nonradiative transition probabilities ($W_{NR}$) of the matrices will influence the rare earth ion emission intensity. The formula for the nonradiative rate is given by the following eqn (3):[41,42]

$$W_{NR} = C\left[\frac{1}{\exp\left(\frac{hw_p}{kT}-1\right)}+1\right]^{\frac{\Delta E}{hw_p}}\exp\left(\frac{\Delta E \ln \varepsilon}{hw_p}\right) \quad (3)$$

where $\Delta E$ is the measure of the relative offset between these levels; $\varepsilon$ accounts for the exact nature of the ion-phonon coupling and is insensitive as $\ln(\varepsilon)$ in the formula; the constant $C$ depends on the phonon density of the matrix. $w_p$ refers to the maximum phonon frequency of the host. It is known that the influence of crystal lattice on the rare earth ion luminescence mainly depends on the phonon.[40] For the sake of discussing the impact of different lattices on the $Eu^{3+}$ emission intensity, eqn (4) is introduced. From Fig. 13, the maximum phonon energy of $AgLu(MoO_4)_2$ and $LiLu(MoO_4)_2$ hosts show no difference, and then the values of $\varepsilon$ and $C$ should only be considered. With regard to the present molybdate matrices, the intensity of ion-phonon coupling ($\varepsilon$) depends on the impact of $Li^+$ or $Ag^+$ on the tetrahedron $[MoO_4]^{2-}$. Due to the difference of the deformation ability of ions mentioned above, the polarization ability of $O^{2-}$ in the tetrahedron $[MoO_4]^{2-}$ to the rare earth $Eu^{3+}$ becomes stronger and the intensity of ion-phonon coupling ($\varepsilon$) is greater in the $AgLu_{0.95}(MoO_4)_2$:0.05$Eu^{3+}$


This journal is © The Royal Society of Chemistry 2015

Published on 16 September 2015. Downloaded by State Public Scientific Technical Library, Siberian Branch of the RAS on 10/19/2020 12:44:16 PM.

system. Furthermore, according to Debye approximation, the following eqn (4) can be achieved:

$$C \propto \rho(w)^{5/3} \quad (4)$$

where $\rho(w)$ is the phonon density of state of the matrix.[43] Thus a larger phonon density will lead to a larger $C$, implying a greater $W_{NR}$ and a weaker $Eu^{3+}$ emission intensity. As shown in Fig. 13, the maximum phonon frequency peak (880 $cm^{-1}$) in the $LiLu(MoO_4)_2$ host material has a smaller area and weaker intensity than that in the $AgLu(MoO_4)_2$ host material. Therefore, the maximum energy phonon density is defined as the specific value of the integrated intensity of the maximum phonon vibration peak and the integrated intensity of the host Raman scattering curve. After calculation, the maximum energy phonon density of $AgLu(MoO_4)_2$ and $LiLu(MoO_4)_2$ are 0.6221 and 0.5597, respectively. Then, the $AgLu(MoO_4)_2$ host has greater values of $\varepsilon$ and $C$ than that of the $LiLu(MoO_4)_2$ host. Based on eqn (4), the nonradiative transition probabilities ($W_{NR}$) in the $AgLu(MoO_4)_2$ are greater than that of $LiLu(MoO_4)_2$, and then it is reasonable to find that the $Eu^{3+}$ emission intensity of the $AgLu_{0.95}(MoO_4)_2$:$0.05Eu^{3+}$ system is weaker than that of $LiLu_{0.95}(MoO_4)_2$:$0.05Eu^{3+}$.

In all, the interpretation has been proposed on the reason that the $Eu^{3+}$ emission intensity of the $AgLu_{0.95}(MoO_4)_2$:$0.05Eu^{3+}$ system is weaker than that of the $LiLu_{0.95}(MoO_4)_2$:$0.05Eu^{3+}$ system. According to Fig. 12, the lower edge of the matrix conduction band is much closer to the excitation band energy level of $Eu^{3+}$ and it may have some kind of coupling which will produce a kind of energy loss (nonradiative transition), leading to diminishing $Eu^{3+}$ emission intensity. As mentioned previously, the $E_g$ values of $AgLu(MoO_4)_2$ and $LiLu(MoO_4)_2$ are 3.08 eV and 3.58 eV, respectively, thus the band gap of the $Li_xAg_{1-x}Lu_{0.95}(MoO_4)_2$:$0.05Eu^{3+}$ will be much closer to the energy level gap 2.67–3.14 eV (394–464 nm) of the activator $Eu^{3+}$ with increasing Ag/Li ratios. As a result, there may be a part of the coupling between two energy levels of $AgLu(MoO_4)_2$ and the activator $Eu^{3+}$. This phenomenon also exists in the $Er^{3+}$ doped molybdate matrix systems.[7] However, since the Li-contained material has a wider band gap than that of the Ag-based material, we can only know the excited state of $Eu^{3+}$ is much closer to the conduction band of $Ag^+$. According to Boltzmann distribution, we can qualitatively know that the excited state electron number of $Eu^{3+}$ distributes more to the conduction band of $Ag^+$, which will cause possible energy loss, leading to the lower $Eu^{3+}$ emission intensity. But we cannot confirm the absolute position of the $Eu^{3+}$ level in the band gaps for the two different kinds materials, thus the specific numerical values of the energy difference between excited state of $Eu^{3+}$ and the conduction band of $Ag^+$ or $Li^+$ is by far unclear. Hence, the energy coupling between the $AgLu(MoO_4)_2$ matrix and $Eu^{3+}$ was weakened when $Li^+$ was introduced into the $Li_xAg_{1-x}Lu_{0.95}(MoO_4)_2$:$0.05Eu^{3+}$ phosphors.

As for the excitation spectra of $Li_xAg_{1-x}Lu_{0.95}(MoO_4)_2$:$0.05Eu^{3+}$ ($x$ = 0.1, 0.3, 0.5, 0.7, 0.9, 1.0) phosphors, both the $^7F_0 \rightarrow {}^5L_6$ transition at 394 nm and $^7F_0 \rightarrow {}^5D_2$ transition at 464 nm, are not only closely related to the energy coupling (the nonradiative transition) but also most associated with the near ultraviolet energy absorption and transmission efficiency between the CT band of $O^{2-}$–$Mo^{6+}$ and the 4f → 4f emissive transitions of $Eu^{3+}$. As a typical rare earth activated photoluminescence process, the electrons in the $Eu^{3+}$ absorb some energy, transferring from the ground state $^7F_0$ to the excited state, then always revert to the original equilibrium state, completing the photoluminescence process. However, the emission process of molybdate matrix luminescent materials is mainly completed through two processes, the electrons in a higher excited state will transfer to the lower excited state $^5D_0$ *via* the energy transfer or nonradiative transitions appear and go back to the ground state $^7F_j$ ($j$ = 0, 1, 2, 3, 4, 5, 6) by coupling of the CT band of $O^{2-}$–$Mo^{6+}$, and another way is through the electron phonon relaxation process of rare earth energy levels, relaxing from a higher excited state to excited state $^5D_0$. Both the processes will finally get back to the ground state $^7F_j$ ($j$ = 0, 1, 2, 3, 4, 5, 6) from excited states $^5D_0$, and the $Eu^{3+}$ emission is achieved. For the $^7F_0 \rightarrow {}^5L_6$ transition and the $^7F_0 \rightarrow {}^5D_2$ transition, the photoluminescence process is mainly through the coupling of the CT band of $O^{2-}$–$Mo^{6+}$, however, this process contains both the energy transfer and energy coupling loss from the CT band of $O^{2-}$–$Mo^{6+}$ to $Eu^{3+}$ energy levels, and the energy loss process will lead to a higher nonradiative transition probability. Thus, *via* composition modulation in the $Li_xAg_{1-x}Lu_{0.95}(MoO_4)_2$:$0.05Eu^{3+}$ ($x$ = 0.1, 0.3, 0.5, 0.7, 0.9, 1.0) phosphors, the PLE and PL intensity of the $Li_{0.8}Ag_{0.2}Lu_{0.95}(MoO_4)_2$:$0.05Eu^{3+}$ phosphor is the strongest one, which is due to the balance of the energy transfer and the coupling nonradiative transition between the CT band of $O^{2-}$–$Mo^{6+}$ and $Eu^{3+}$ energy levels.

## 4. Conclusion

In conclusion, the double molybdate solid-solution phosphors $Li_{1-x}Ag_xLu_{1-y}(MoO_4)_2$:$yEu^{3+}$ were designed and reported in this paper. The crystal structure and phase formation of the $Li_{1-x}Ag_xLu_{1-y}(MoO_4)_2$:$yEu^{3+}$ solid solutions were discussed in detail. With increasing Li/Ag ratios, the nonradiative transition between two energy levels of the $Li_xAg_{1-x}Lu(MoO_4)_2$ host and the activator $Eu^{3+}$ has been weakened since the band gaps of the host were enlarged, and then the $Eu^{3+}$ emission intensities were enhanced. A model on the evaluation of the polarization ability of cations has been built to explore the relationship between the $Eu^{3+}$ energy level and the host. The luminescence intensity of molybdate matrix materials is not only related to the coupling nonradiative transition probabilities of the phonons but also associated with near ultraviolet energy absorption and transmission efficiency between the CT band of $O^{2-}$–$Mo^{6+}$ and the 4f → 4f emissive transitions of $Eu^{3+}$. These results could shed light on the research and understanding of luminescence intensity and efficiency enhancement in $Eu^{3+}$ doped luminescent materials.

Published on 16 September 2015. Downloaded by State Public Scientific Technical Library, Siberian Branch of the RAS on 10/19/2020 12:44:16 PM.

## Acknowledgements

The present work was supported by the National Natural Science Foundations of China (Grant No. 51272242, 51572023, 51511130035), Natural Science Foundations of Beijing (2132050), the Program for New Century Excellent Talents in University of Ministry of Education of China (NCET-12-0950), Beijing Nova Program (Z131103000413047), Beijing Youth Excellent Talent Program (YETP0635), the Funds of the State Key Laboratory of Rare Earth Resource Utilization, Changchun Institute of Applied Chemistry, Chinese Academy of Sciences (RERU2015022), and the excellent tutor section of the Fundamental Research Funds for the Central Universities of China University of Geosciences, Beijing (2-9-2015-028). This work was also partly supported by the Russian Foundation for Basic Research (Grant No. 15-52-53080 GFEN_a).

## Notes and references

1 P. V. Klevtsov and R. F. Klevtsova, *J. Struct. Chem.*, 1977, **18**, 339–355.
2 V. A. Morozov, A. Bertha, K. W. Meert, S. V. Rompaey, D. Batuk, G. T. Martinez, S. V. Aert, P. F. Smet, M. V. Raskina, D. Poelman, A. M. Abakumov and J. Hadermann, *Chem. Mater.*, 2013, **25**, 4387–4395.
3 H. Y. Li, S. Y. Zhang, S. H. Zhou, X. Q. Cao and Y. H. Zheng, *J. Phys. Chem. C*, 2009, **113**, 13115–13120.
4 H. Y. Li, H. K. Yang, B. K. Moon, B. C. Choi, J. H. Jeong, K. Jang, H. S. Lee and S. S. Yi, *Inorg. Chem.*, 2011, **50**, 12522–12530.
5 V. Sivakumar and U. V. Varadaraju, *J. Electrochem. Soc.*, 2006, **153**, H54–H57.
6 S. Neeraj, N. Kijima and A. K. Cheetham, *Chem. Phys. Lett.*, 2004, **387**, 2–6.
7 F. R. Cheng, Z. G. Xia, X. P. Jing and Z. Y. Wang, *Phys. Chem. Chem. Phys.*, 2015, **17**, 3689–3696.
8 J. G. Wang, X. P. Jing, C. H. Yan and J. H. Lin, $Ca_{1-2x}Eu_xLi_xMoO_4$: a novel red phosphor for solid-state lighting based on a GaN LED, *J. Electrochem. Soc.*, 2005, **152**, G186–G188.
9 J. Liu, H. Z. Lian and C. S. Shi, *Opt. Mater.*, 2007, **29**, 1591–1594.
10 X. G. Liu, L. Li, H. M. Noh, J. H. Jeong, K. Jang and D. S. Shinc, *RSC Adv.*, 2015, **5**, 9441–9454.
11 L. L. Li, J. J. Zhang, W. W. Zi, S. C. Gan, G. J. Ji, H. F. Zou and X. C. Xu, *Solid State Sci.*, 2014, **29**, 58–65.
12 S. Ye, C. H. Wang and X. P. Jing, *J. Electrochem. Soc.*, 2008, **155**, J148–J151.
13 S. Ye, C. H. Wang, Z. S. Liu, J. Lu and X. P. Jing, *Appl. Phys. B*, 2008, **91**, 551–557.
14 S. Ye, C. H. Wang and X. P. Jing, *J. Electrochem. Soc.*, 2009, **156**, J121–J124.
15 C. C. Zhao, X. Yin, F. Q. Huang and Y. Hang, *J. Solid State Chem.*, 2011, **184**, 3190–3194.
16 C. H. Chiu, M. F. Wang, C. S. Lee and T. M. Chen, *J. Solid State Chem.*, 2007, **180**, 619–627.
17 C. F. Guo, S. T. Wang, T. Chen, L. Luan and Y. Xu, *Appl. Phys. A: Mater. Sci. Process.*, 2009, **94**, 365–371.
18 A. V. Zaushutsyn, V. V. Mikhailin, A. Y. Romanenko, E. G. Khaikina, O. M. Basovich, V. A. Morozov and B. I. Lazoryak, *Inorg. Mater.*, 2005, **41**, 766–770.
19 O. D. Chimitova, V. V. Atuchin, B. G. Bazarov, M. S. Molokeev and Z. G. Bazarova, *SPIE Proc.*, 2013, **8771**, 87711A.
20 Bruker AXS, *TOPAS V4: General profile and structure analysis software for powder diffraction data. – User's Manual*, Bruker AXS, Karlsruhe, Germany, 2008.
21 V. A. Efremov, N. D. Zakharov, G. M. Kuz'micheva, B. V. Mukhin and V. V. Chernyshev, *Russ. J. Inorg. Chem.*, 1993, **38**, 203–207.
22 V. Sivakumar and U. V. Varadaraju, *J. Electrochem. Soc.*, 2005, **152**, H168–H171.
23 P. Dorenbos, *J. Phys.: Condens. Matter*, 2003, **15**, 8417–8434.
24 Q. L. Dai, H. W. Song, G. H. Pan, X. Bai, H. Zhang, R. F. Qin, L. Y. Hu, H. F. Zhao, S. Z. Lu and X. G. Ren, *J. Appl. Phys.*, 2007, **102**, 054311.
25 Q. L. Dai, H. W. Song, X. Bai, H. Zhang, R. F. Qin, L. Y. Hu, H. F. Zhao, S. Z. Lu and X. G. Ren, *J. Phys. Chem. C*, 2007, **111**, 7586–7592.
26 H. J. Jin, H. Wu and L. H. Tian, *J. Lumin.*, 2012, **132**, 1188–1191.
27 V. A. Morozov, A. V. Arakcheeva, P. Pattison, K. W. Meert, P. F. Smet, D. Poelman, N. Gauquelin, J. Verbeeck, A. M. Abakumov and J. Hadermann, *Chem. Mater.*, 2015, **27**, 5519–5530.
28 L. L. Li, J. J. Zhang, W. W. Zi, S. C. Gan, G. J. Ji, H. F. Zou and X. C. Xu, *Solid State Sci.*, 2014, **29**, 58–65.
29 K. Binneman and C. Görller-Walrand, *J. Rare Earths*, 1996, **14**, 173–180.
30 G. L. Miessler and D. A. Tarr, *Inorg. Chem.*, Pearson Press, US, Inter. 4th edn, 2011, p. 718.
31 J. Pankove, *Opt. Processes in Semiconductors*, Prentice-Hall, Inc., Upper Saddle River, NJ, 1971, p. 34.
32 J. Hao and M. Cocivera, *J. Phys. D: Appl. Phys.*, 2002, **35**, 433–438.
33 P. W. Atkins, T. L. Overton, J. P. Rourke, M. T. Weller and F. A. Armstrong, *Inorg. Chem*, Oxford University Press, New York, 5th edn, 2010, p. 16.
34 S. Shionoya and W. M. Yen, *Phosphor Handbook*, CRC Press, New York, 1998, 163.
35 H. Fuks, S. M. Kaczmareka, G. Leniec, L. Macalik, B. Macalik and J. Hanuza, *Opt. Mater.*, 2010, **32**, 1560–1567.
36 K. Huang and A. Rhys, *Proc. R. Soc. London, Ser. A*, 1950, **204**, 406–423.
37 K. Huang, *Contemp. Phys.*, 1981, **22**, 599–612.
38 Z. Pan, J. P. Wicksted and H. Liu, *Phys. Rev. B: Condens. Matter*, 1993, **48**, 844–852.
39 L. A. Riseberg and M. J. Weber, in *Progress in Optics, XIV*, ed. E. Wolf, Elsevier, North-Holland, 1976, ch. III.

 This journal is © The Royal Society of Chemistry 2015

View Article Online



Published on 16 September 2015. Downloaded by State Public Scientific Technical Library, Siberian Branch of the RAS on 10/19/2020 12:44:16 PM.

40 Z. Pan, S. H. Morgan, A. Loper, V. King, B. H. Long and W. E. Collins, *J. Appl. Phys.*, 1995, **77**, 4688–4692.
41 D. C. Yeh, W. A. Sibley, M. Suscavage and M. G. Drexhage, *J. Appl. Phys.*, 1987, **62**, 266–275.
42 B. Layne, W. H. Lowdermilk and M. Weber, *Phys. Rev. B: Solid State*, 1977, **16**, 3259–3261.
43 R. C. Powell, *Phys. Solid-State Laser Mater.*, Springer Press, NewYork, 1998, ch. 4.

This journal is © The Royal Society of Chemistry 2015